SmtB−DNA and Protein−Protein Interactions in the Formation of the Cyanobacterial Metallothionein Repression Complex: Zn^{2+} Does Not Dissociate the Protein−DNA Complex in Vitro†

Sambit R. Kar,‡ Jacob Lebowitz,*,‡,§ Scott Blume,|| Kenneth B. Taylor,⊥ and Leo M. Hall⊥

Graduate Program in Biophysical Sciences, Department of Medicine, Department of Microbiology, and Department of Biochemistry and Molecular Genetics, University of Alabama at Birmingham, Birmingham, Alabama 35294, and Division of Bioengineering and Physical Science, National Institutes of Health, Bethesda, Maryland 20892

Received June 20, 2001; Revised Manuscript Received August 24, 2001

ABSTRACT: The synechococcal metallothionein locus *smt* consists of two divergent genes: *smtA* coding for the metallothionein SmtA, and *smtB* coding for the trans-acting regulator SmtB. The latter binds at two inverted repeats, designated S1/S2 and S3/S4, in the overlapping promoter/operator sites between the two genes. We have determined the binding stoichiometries to the entire operator/promoter DNA and to the separate S1/S2 and S3/S4 half-operator oligonucletides using sedimentation equilibrium and sedimentation velocity measurements. The full promoter/operator DNA binds two SmtB dimers. The hydrodynamic behavior of this complex supports a compact nucleoprotein structure. Each separate S1/S2 and S3/S4 operator sequence also binds two dimers. An equal molar mixture of separate S1/S2 and S3/S4 operator sequences, in excess SmtB, forms a S1/S2−SmtB:SmtB−S3/S4 bridge complex. Combining these results with previously published binding interference data, which showed consecutive S1/S2 and S3/S4 SmtB occupancy on the operator/promoter DNA, we have developed a model for the establishment of the repression complex that appears to involve significant DNA compaction, presumably DNA bending, stabilized by SmtB−SmtB bridge interactions. DNase I footprinting titrations also showed consecutive S1/S2 and S3/S4 SmtB occupancy. The footprints expand considerably in the presence of Zn^{2+}. Hence, SmtB remains bound to the operator sites when Zn^{2+} ions are present. This result is further supported by gel retardation assay. Failure of the metal ions to dissociate SmtB from the DNA points to a hitherto unknown function of SmtB in the regulation of the *smt* locus.

In *Synechococcus* PCC7942, Zn^{2+} and Cd^{2+} homeostasis is maintained by the *smt* locus of the chromosome (*1*). This locus consists of two divergently transcribed genes, *smtA* and *smtB* (Figure 1A). The former encodes SmtA,[1] a class II metallothionein. The latter encodes SmtB, a putative trans-acting repressor of *smtA*. A 100 bp operator/promoter region lies between the *smtA* and the *smtB* protein coding regions, and contains divergent overlapping promoters for the two genes (*1*). The promoter for *smtA* contains a pair of template/nontemplate sites, respectively designated S1 and S2, within an imperfect 6-2-6 inverted repeat near the *smtA* transcription start site (Figure 1). Another pair of sites, designated S3 and S4, is situated within a 7-2-7 inverted repeat between the −10 sequences of the two divergent genes (Figure 1). Both pairs of sites are contacted by SmtB at a TGAA sequence as deduced from methylation interference assays (*2*). In the absence of metal ions, the transcription of *smtA* is repressed while the transcription is enhanced in response to increased concentrations of Zn^{2+} and Cd^{2+}, and to lesser extent by Cu^{2+}, Hg^{2+}, Co^{2+}, Ni^{2+}, Au^{2+}, and Ag^{+} ions (*3*, *4*).

It has recently been shown that recombinant SmtB exists in solution in a monomer−dimer−tetramer equilibrium with the dimer being the predominant form. Hydrodynamic analysis suggests that the dimeric protein is significantly asymmetric (*5*). When the protein binds Zn^{2+} ions, it not only exhibits stronger dimerization, but also changes conformation as well, and becomes significantly more compact (*5*). The

† This work was supported in part by XL-A Instrumentation Grant BIR-9419624 from the National Science Foundation to J.L., by the National Oceanic and Atmospheric Administration, US Department of Commerce, under Grant NA016RG0155, Project E/0-16, and by the Mississippi−Alabama Sea Grant Consortium to L.M.H. and K.B.T.

* Correspondence should be addressed to this author at the Molecular Interactions Resource, Division of Bioengineering and Physical Science, ORS, National Institutes of Health, Building 13, Room 3N17, Office Building 13, Room 3E49, 13 South Dr., Bethesda, MD 20892-5766. Tel: (301) 435-1955, Fax: (301) 480-1242, E-mail: lebowitz@helix.nih.gov.

‡ Graduate Program in Biophysical Sciences, University of Alabama at Birmingham, and Division of Bioengineering and Physical Science, NIH.

§ Department of Microbiology.

|| Department of Medicine, University of Alabama at Birmingham.

⊥ Department of Biochemistry and Molecular Genetics, University of Alabama at Birmingham.

[1] Abbreviations: SmtA and SmtB, synechococcal metallothionein locus gene products; bp, base pair; HTH, helix−turn−helix; NTA, nitrilotriacetic acid; Tris, tris(hydroxymethyl)aminomethane; DTT, dithiothreitol; EDTA, ethylenediaminetetraacetic acid; TBE, Tris, borate, EDTA buffer; EMSA, electrophoretic mobility shift assay(s); S.D., Shine−Delgarno sequence; T.S., transcription start site(s); mMT1, mouse metallothionein; RASMB, reversible associations in structural and molecular biology; CAP, catabolite gene activator protein; HNF-3, hepatocyte nuclear factor-3.

10.1021/bi011289f CCC: $20.00
Published on Web 10/04/2001

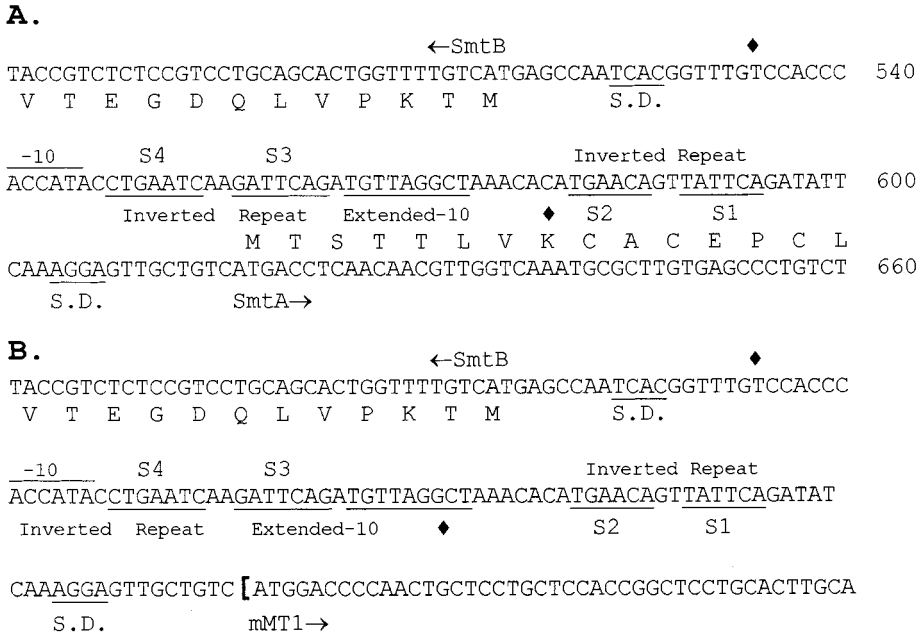

FIGURE 1: *smt* locus. (A) Nucleotide sequence of part of the *smt* locus of *Synechococcus* PCC7942, showing only the template strand (with respect to *smtB*). The nucleotide sequence is according to Huckle et al. (*3*). The diamonds mark the transcriptional start sites for the two genes. The inverted repeat sequences where SmtB binds [contact interactions with the G residue of sequence motif TGAA (see text)] are shown, and the half-sites S1 (complementary strand) and S2 (strand shown) and S3 (complementary strand) and S4 (strand shown) are indicated. The features of the operator/promoter region are marked and annotated. S.D. stands for Shine−Delgarno sequences. (B) Corresponding fragment of the plasmid pJLE3C in which the *mMT1* gene replaces the *smtA* gene (the coding region begins at the left bracket). This fragment has been used in the footprinting assay shown in Figure 6.

X-ray crystallographic structure of SmtB is in complete agreement with these observations in that the protein crystallizes as a dimer with two putative "winged" helix−turn−helix (HTH) DNA binding domains, one in each subunit (*6*). The structure shows SmtB to be an elongated dimer with approximate dimensions of 20 Å × 30 Å × 68 Å. Analysis of a mercuric acetate derivative of the crystal shows four putative metal ion binding sites in the dimer, two sites at the DNA binding domains, and two more at the dimer interface consisting of residues from both subunits (*6*). The apparent agreement between the number of mercuric binding sites and the equilibrium dialysis determination of Zn^{2+} binding sites using $^{65}ZnCl_2$ (*5*) suggested that the crystallographic Hg^{2+} and the Zn^{2+} binding sites were identical. However, it has been very recently shown by optical spectroscopy that there is only one very high affinity Zn^{2+} binding site per monomer with an association constant in excess of 10^{11} M^{-1} (*7*). The latter study also pointed out that the equilibrium dialysis data of Kar et al. (*5*) were not corrected for the presence of nitrilotriacetic acid (NTA), which would act as binding competitor for Zn^{2+}. When the equilibrium dialysis data were reanalyzed by taking into consideration NTA binding competition for Zn^{2+}, SmtB was found to have only one high-affinity site per monomer (*7*). Preliminary NMR results suggest that Cys14 in the N-terminal flexible region is part of a ligand binding site for Zn^{2+} (*8*).

Recombinant SmtB forms three distinct gel retardation protein−DNA complexes in vitro with the operator/promoter DNA as a function of SmtB concentration (*1*, *2*). These protein−DNA complexes have been designated C1, C2, and C3 in order of decreasing electrophoretic mobility and in order of appearance with increasing SmtB concentration. Simultaneous to the formation of C3, the formation of C1 and C2 is decreased until finally only C3 is observed. Guanine methylation binding interference assays, using dimethyl sulfate, were used to identify the SmtB binding sites for each complex (*2*). The DNA from isolated complexes identifies those DNA molecules with modified G residues that interfere with binding. The fastest migrating complex C1 binds SmtB at either S1 or S2 or both since methylation of the G residue of the TGAA sequence at the S1 or the S2 site partially interferes with binding (Figure 1A). In the intermediate complex C2, both the S1 and S2 sites are contacted by SmtB. In addition, modification of the G residue in S3 partially interferes with C2 complex formation. At saturating protein concentrations, both S1/S2 and S3/S4 are bound by SmtB in the slowest migrating complex C3, since methylated G residues in either S1/S2 or S3/S4 inhibit C3 complex formation. These data support both a sequential mode of SmtB binding to the two pairs of sites and a linkage between the two sites since modification of any of the G residues contacted by SmtB completely destabilizes the C3 complex. The formation of all three DNA−protein complexes is inhibited in vitro by Zn^{2+} ions (*2*). However, for the latter experiments, Zn^{2+} ions were added to SmtB before the addition of DNA.

The present study has been undertaken to further understand the sequential steps of SmtB binding leading to the final repression complex. Binding stoichiometries of SmtB were determined for the entire operator/promoter DNA and as well as for oligonucleotides containing either the S1/S2 or the S3/S4 sites separately. Sedimentation velocity binding titrations established the conditions for binding saturation and provided the approximate hydrodynamic shapes of the respective SmtB−DNA complexes. By combining the sedimentation, electrophoretic, and binding interference results, a working model of the SmtB binding interactions has been

developed for the steps that lead to a functional repression complex.

In the literature, it has been assumed that the DNA-bound SmtB, upon binding metal ions, would dissociate from the DNA, leading to de-repression of the metallothionein gene (*1*, *9*, *10*). However, it has never been experimentally shown that the metal ions actually cause dissociation of the protein−DNA complexes. We have investigated the effects of Zn^{2+} on the SmtB−operator/promoter complex with unexpected results. The addition of Zn^{2+} causes an expansion of the footprint protection patterns rather than abolishing them. Likewise, the C3 complex remains unaffected by the addition of Zn^{2+} in the gel shift assay. Whereas Zn^{2+} binding causes free SmtB to change its overall conformation (*5*), rendering it incapable of binding DNA, this is not the case for SmtB bound to operator/promoter DNA.

MATERIALS AND METHODS

Chemicals and Molecular Biology Materials. Tris(hydroxymethyl)aminomethane (Tris), dithiothreitol (DTT), and ethylenediaminetetraacetic acid (EDTA) were from Fisher Scientific. $ZnCl_2$ was bought from Mallinckrodt, Inc. Other reagent grade chemicals were from Sigma or Fisher Scientific. The S1/S2 (32 bp), the S3/S4 (31 bp), and the operator/promoter (100 bp) oligonucleotides have been obtained from IDT, Inc. Molecular weights of the respective duplexes are 20 800, 20 150, and 65 000 as determined by mass spectrometric analysis performed by the vendor. VivaSpin15 membrane filtration units were from VivaScience. The Klenow fragment of DNA polymerase I and the restriction endonuclease *Pst*I were purchased from Gibco BRL while the restriction endonuclease *Bsr*FI was from New England Biolabs, Inc. α-[^{32}P]dCTP is from Amersham. Recombinant SmtB has been expressed and purified according to published protocols (*5*). No attempt was made to determine whether the SmtB preparation contained a fraction of molecules that were incompetent to bind DNA. However, the footprint and gel retardation complexes are formed in the 50 nM range, suggesting that the amount of binding-incompetent SmtB is low (see Results).

SmtB Concentration Designation for the Respective Binding Analyses Reported Below. The molar extinction coefficient of monomer SmtB at 280 nm, 5960 M^{-1} cm^{-1}, was used to measure the concentration of purified SmtB (*5*). As discussed above, SmtB monomers, dimers, and tetramers are in reversible equilibrium, with dimers being predominant. We express the addition of SmtB in terms of monomer concentration for all the reported results with the exception of the band titration for the generation of a binding isotherm in terms of added dimer concentration. The latter was calculated based on the association constants that we previously determined (*5*).

Titration of the 100 bp Operator/Promoter DNA with SmtB by Band Velocity Sedimentation. Binding of SmtB to the entire operator/promoter DNA has been monitored by the band sedimentation technique in the XL-A using Type III centerpieces (*11*) in a four-cell An-60 Ti rotor. A 2 μM sample of the DNA has been titrated with increasing concentrations of protein (from 0 to 40 μM monomer). Twenty-five microliters of the DNA−protein mixture (preincubated for 1 h) in 25 mM Tris, 2 mM DTT, 2 mM EDTA, 0.1 M NaCl, pH 7.4, was layered onto a sector solution column of 50% buffered D_2O in each cell of the rotor, centrifuged at 58 000 rpm and 20 °C, and the moving band was monitored at 250 nm where the protein absorbance is insignificant. Each titration point was measured in triplicate, and the average *s* value was plotted vs the total dimer concentration (Figure 3).

Titration of S1/S2 and S3/S4 Oligonucleotides with SmtB by Boundary Velocity Sedimentation. The boundary sedimentation velocity technique has been used to monitor the binding of SmtB to the S1/S2 and the S3/S4 oligonucleotides. Sedimentation has been done in a Beckman XL-A Analytical Ultracentrifuge using a four-cell An-60 Ti rotor at a speed of 54 000 rpm, and data were collected at 250 nm, at which the absorption by SmtB is insignificant. Then a 1.5 μM aliquot of each oligonucleotide was titrated with increasing concentrations of SmtB (from 0 to 30 μM monomer) in 25 mM Tris, 2 mM DTT, 2 mM EDTA, 0.1 M NaCl, pH 7.4, 22 °C. The data have been analyzed by the time-derivative *g*[*s**] method developed by Stafford (*12*). The *g*[*s**] analysis for each titration point has then been superimposed to generate the composites shown in Figure 4A,B.

Aliquots of the protein were added to the same DNA−protein mixture in the centrifuge cell, and the cell was shaken up to mix the components well after each run, equilibrated for 1 h, and centrifuged again. This results in progressive dilution of the DNA while the final protein concentrations are the ones indicated in the inset of each figure, hence the diminishing peak heights of the DNA signal for each titration step.

Hydrodynamic Calculations. One can predict the sedimentation velocity coefficients for smooth spherical proteins or protein complexes by combining the Svedberg equation and Stokes equation for the frictional coefficient to obtain eq 1:

$$s = 0.12\frac{M(1 - \bar{v}_{\text{protein}}\rho)}{\bar{v}^{1/3}} \qquad (1)$$

where M equals the molecular weight and $\bar{v}_{\text{protein}}$ and ρ are the partial specific volume of the protein and the density of water, respectively. The spherical shape *s* value from eq 1 is the maximum *s* value that can be obtained for the given M value of the protein or protein complex with a corresponding minimum frictional coefficient, f_o. The ratio of the experimental frictional coefficient (f) to the minimum frictional coefficient (f/f_o), which is equivalent to $s_{max}/s_{20,w}$, measures the maximum total shape asymmetry of the protein. The total shape asymmetry f/f_0 can be separated into two factors, a geometrical shape asymmetry and a hydration expansion, and this formulation is given by eq 2.

$$\frac{f}{f_0} = \frac{f}{f_{\text{shape}}}\left(\frac{1 - \delta\bar{v}_1}{\bar{v}_2}\right)^{1/3} \qquad (2)$$

Partial specific volume subscripts 1 and 2 designate water and the protein or protein complex, respectively, and δ is the hydration in grams of water per gram of protein. Using f/f_o or f/f_{shape} values, one can model a protein or protein complex with different ellipsoid shapes. This modeling can be rapidly accomplished using the public domain software program Sednterp (http://www.bbri.org/RASMB/rasmb.html). In

this program, the semimajor to semiminor (a/b) axial ratio of a prolate or oblate ellipsoid of revolution is determined using respective power series approximation of the tabulated data for a/b as a function of ($f/f_o - 1$) or ($f/f_{shape} - 1$) for each ellipsoid. One needs to designate a δ value for Sednterp to calculate the f/f_{shape} to be used in the power series approximation to obtain axial ratios of ellipsoids.

Determination of Stoichiometries of SmtB Binding to the Different Oligonucleotides by Equilibrium Sedimentation. Sedimentation equilibrium analysis has been performed in the XL-A Analytical Ultracentrifuge using a four-cell An-60 Ti rotor. Mixtures of each oligonucleotide with 40-times molar excess of SmtB over DNA were centrifuged at 8000 rpm and data gathered at 250 nm. At this wavelength, there is no optical contribution from protein absorbance, and only the absorbance from DNA is detected. At binding saturation, the optical signal will represent only protein−DNA complexes. The molar concentration ratio of SmtB to DNA used was 2-fold the molar ratio needed to reach saturation in the sedimentation velocity binding titrations described above. For the stoichiometric analysis of binding to the S1/S2 and S3/S4 oligonucleotides, a DNA concentration of 0.35 μM was used, respectively. For the stoichiometric analysis of binding of SmtB to the operator/promoter DNA, the concentration of DNA was 0.2 μM. The interaction of SmtB with both the S1/S2 and the S3/S4 oligonucleotides simultaneously was analyzed by equilibrium sedimentation of an equimolar mixture of the two oligonucleotides (total concentration 0.35 μM) with 40 times molar excess of SmtB over DNA at 8000 rpm. Equilibrium is considered reached when two consecutive sets of data taken 2 h apart are completely superimposable with small RMS difference and the difference spectra show no systematic deviations (Figure 2A−C).

For a single ideal component or complex at sedimentation equilibrium, the total solute concentration at any radial position r is given by the following expression: $C_r = (C_{ref})\exp[M(1 - \nu_{bar}\rho)(\omega^2)(r^2 - r_{ref}^2)/2RT]$ where C_{ref} is the concentration at a reference position, M is the weight average molecular weight of the macromolecular complex, ν_{bar} is the partial specific volume of the complex, ω is the density of the sedimentation solvent, ρ is the angular velocity, R is the gas constant, and T is the temperature in degrees kelvin. The sedimentation equilibrium data for each DNA−protein mixture under saturating conditions have been fitted by a nonlinear least-squares method to the distribution of a single species to estimate the weight average molecular weight of the complex (*13*). From that estimated molecular weight, subtraction of the molecular weight of the DNA fragment yields the mass of the protein associated with the DNA (*13*). To determine the molecular weights of SmtB−DNA complexes, we need to estimate the respective partial specific volumes of the saturated protein−DNA complex under examination. The partial specific volume of a protein−DNA complex is equal to the weight fraction of the protein times its partial specific volume plus the weight fraction of the DNA times its partial specific volume. This relationship, upon algebraic manipulation, yields eq 3:

$$\bar{v}_{complex} = \frac{\bar{v}_{DNA} + R\bar{v}_{protein}}{1 + R} \qquad (3)$$

where $\bar{v}_{protein}$ and $\bar{v}_{DNA}$ are the respective partial specific volume of protein and DNA and R is the ratio of the mass of the protein to that of the DNA in a complex. The partial specific volume of SmtB is 0.734 $cm^3 \cdot g^{-1}$ (*5*) while that of each duplex oligonucleotide has been calculated based on its individual guanine plus cytosine content (*14*). The partial specific volume of DNA calculated by these authors has been based on tabulated data from experiments using CsCl. The high ionic strength conditions may slightly shift the observed values compared to those obtained using the buffers described for the current experiments. The G+C contents of the S1/S2, the S3/S4, and the operator/promoter DNA are 34.4%, 41.9%, and 43%, respectively. Thus, the respective partial specific volumes for the oligonucleotides were calculated to be 0.592, 0.590, and 0.589 $cm^3 \cdot g^{-1}$, respectively. For 1:2 DNA−dimer complexes with each of the three oligonucleotides, the values for R are 2.579, 2.662, and 0.825, respectively. The partial specific volumes for the complexes can then be calculated to be 0.694, 0.695, and 0.655 $cm^3 \cdot g^{-1}$, respectively, assuming there is no significant volume change upon protein binding the DNA.

DNase I Footprint and Electrophoretic Mobility Shift Assays. The DNase I footprint of the repressor on the operator/promoter DNA was obtained in vitro using a 141 bp *Bsr*FI−*Pst*I fragment from the plasmid pJLE3C (*2*). This plasmid contains the repressor gene *smtB*, the entire operator/promoter region of the *smt* locus, and the mouse metallothionein gene *mMT1* in place of the *smtA* gene (Figure 1B). The generated DNA fragment encompasses the first six codons of the *smtB* gene at the *Pst*I restriction end, the entire 100 bp operator/promoter region, and the first seven codons of the *mMT1* at the *Bsr*FI restriction end. The sequence of this fragment has also been verified by automated DNA sequencing (results not shown). The 5′-overhang at the *Bsr*FI restriction site was filled in with α-[^{32}P]dCTP using the Klenow subfragment of the DNA polymerase I to radio-label the template strand (with respect to *smtB*). The preparation of this fragment has been done as per standard protocols (*15*).

The DNase I footprinting was performed with a ∼40 nM aliquot of this DNA fragment with increasing concentrations of SmtB (from 0 to 7.5 μM) according to standard protocols (*15*, *16*). Similar protocols were used to investigate the effect of increasing concentrations of Zn^{2+} (0−50 μM) on the footprint at saturating protein concentration (7.5 μM).

To demonstrate the formation of SmtB−DNA complexes (in the absence of Zn^{2+}), electrophoretic mobility shift assays (EMSA) were done with 2 μL aliquots of the same samples used for DNase I footprinting in the presence of increasing concentrations of SmtB. These reactions were prepared in 20 μL of a solution containing 25 mM Tris-HCl (pH 7.5), 1 mM DTT, and 1 mM EDTA. Then 40 nM ^{32}P-labeled operator/promoter DNA was incubated with various concentrations of SmtB (0−7.5 μM) for 2 h, followed by addition of loading buffer to adjust the glycerol concentration to 5%. Aliquots were electrophoresed at room temperature, at 160 V, on a 10 × 10 cm 6% polyacrylamide gel using a running TBE buffer containing 89 mM Tris, 89 mM boric acid, and 1.56 mM Na_2EDTA (pH 8.0).

To determine the effect of Zn^{2+} on the preformed SmtB−DNA complex C3, a mixture of 18 μL of 25 mM Tris-HCl (pH 7.5), 7.5 μM SmtB, 40 nM ^{32}P-labeled operator/promoter DNA, and 1 mM DTT was incubated at room temperature.

After 2 h, 2 μL aliquots of $ZnCl_2$ from 0 to 0.1 mM were added, and incubation was continued for another 2 h. After addition of loading buffer to adjust glycerol to 5%, the mixtures were electrophoresed on a 10 × 10 cm 6% polyacrylamide gel using TBE in which sodium acetate was substituted for EDTA at an equimolar concentration. Following electrophoresis at 160 V and 4 °C, the bands on the gels were detected by conventional autoradiography.

RESULTS

Determination of the Stoichiometries of SmtB−DNA Complexes. As discussed in the introduction, a sequential binding mechanism appears to occur in the binding occupancy of the SmtB operator/promoter based on gel retardation data and binding interference analysis. However, the binding steps leading to S1/S2 and S3/S4 operator site occupancy have not been elucidated. To characterize the SmtB−operator/promoter binding interactions, we have determined the stoichiometry for SmtB binding to the operator/promoter DNA, as well as to DNA fragments containing the two half-sites (S1/S2 and S3/S4) separately. Although the sedimentation coefficient of the protein−DNA complex at binding saturation, as determined from a sedimentation velocity binding titration, can provide an estimate of the stoichiometry of the final complex, this approach may be complicated by hydrodynamic considerations, i.e., the shape of the complex. In contrast, sedimentation equilibrium analysis offers a rigorous method to determine the stoichiometries of the components in the final respective complexes without hydrodynamic considerations. Obviously, knowledge of the binding stoichiometry allows for a more definitive interpretation of the sedimentation velocity data (see below). As mentioned under Materials and Methods, the low extinction coefficient of SmtB makes it possible to detect almost exclusively the optical signal from DNA at 250 nm. Hence, at saturation of DNA by SmtB, the absorbance as a function of radial position determines the molecular weight of the protein−DNA complex; i.e., the data can be modeled as a single component as discussed under Materials and Methods (*13*). For the operator/promoter DNA (0.2 μM), in the presence of 40-fold molar excess SmtB, the sedimentation equilibrium absorbance (DNA optical signal) vs radial position data (Figure 2A) give a very good fit to a single DNA−protein complex of weight average molecular weight 116 460, which represents a binding stoichiometry of 1.92 SmtB dimers to each 100 bp operator/promoter duplex (Table 1).

For S1/S2 DNA (0.35 μM), in the presence of 40-fold molar excess SmtB, the sedimentation equilibrium concentration vs radial position profile (Figure 2B) gives a weight average molecular weight of 71 771, which represents a binding stoichiometry of 1.90 SmtB dimers per S1/S2 duplex (Table 1).

The sedimentation equilibrium concentration vs radial position profile (Figure 2C) for S3/S4 DNA (0.35 μM), in the presence of 40-fold molar excess SmtB, gives a weight average molecular weight of 70 458, which represents a binding stoichiometry of 1.88 SmtB dimers for every S3/S4 duplex (Table 1).

Summarizing the stoichiometric results (Table 1), the entire promoter/operator forms a 1:2 DNA−dimer complex. Since there are two operator sites, the occupancy is one dimer per operator site. However, both the S1/S2 and S3/S4 half-site oligonucleotides also form 1:2 DNA−dimer complexes (2 dimers per operator site) at SmtB saturation. To attempt to understand the sequential steps leading to final complex formation, we now consider binding of SmtB to target DNA molecules as monitored by sedimentation velocity methodologies.

Band Sedimentation Velocity Titration of SmtB Binding to the Complete Operator/Promoter DNA. The determination of the change in sedimentation velocity of a target DNA as function of increasing concentrations of a binding protein, using either band or boundary methodologies, provides for a possible dissection of binding steps as well as hydrodynamic characterization that can be used to estimate stoichiometry and the shape of the final complex at binding saturation. The binding isotherm (Figure 3) for the interaction of SmtB with the 100 bp operator/promoter oligonucleotide has been generated by band sedimentation velocity analysis of a titration of 2 μM of the oligonucleotide with increasing concentrations of SmtB dimer (0−30.32 μM).

In the above titration, the experimental *s* value increases from 3.69 S (DNA alone) to 6.53 S (DNA−protein complex close to saturation). A sigmoidal fit of the titration data estimates the plateau value at 6.80 S. Upon correcting for the effects of the density and the viscosity of 50% buffered D_2O (*17*), we obtain an $s_{20,w}$ value of 8.52 S near saturation using the final data point at 6.53 S. If the 1:2 DNA−SmtB complex with a molar mass of 118 640 Da and partial specific volume of 0.655 were spherical, the $s_{20,w}$ value would be 11.42 S. The ratio of the spherical $s_{20,w}$ to the experimental $s_{20,w}$ yields a frictional asymmetry of 1.34 (Table 2) and allows us to hydrodynamically model the SmtB−operator/promoter complex from the f/f_o value as discussed under Materials and Methods. We assume that a prolate ellipsoid represents a reasonable model for the complex, and using a δ value of 0.3 g of water per gram of complex, we obtain major and minor axial dimensions of 18.35 and 4.43 nm, respectively, for the ellipsoid. The length of prolate complex can be compared to the full length of the DNA of 34 nm. There appears to be a very significant compaction of DNA in the promoter/operator complex. The compaction may be more significant since we conservatively selected the last data point of Figure 3 and did not use the extrapolated *s* value. Furthermore, if we had allowed for protein roughness or rugosity (*18*, *19*), then the theoretical spherical $s_{20,w}$ value would decrease to 9.55 S and the f/f_o would be only 1.12, which would give essentially a spherical shape with a δ value of 0.3.

To develop a reasonable interpretation of binding steps, it is necessary to determine all species in equilibrium. To attempt to simplify this problem, we examine SmtB binding to the S1/S2 and S3/S4 operator sites separately as discussed below.

Boundary Sedimentation Analysis of SmtB Binding to the S1/S2 Half-Operator/Promoter. Changes in boundary sedimentation velocity have been used to monitor binding of SmtB to the S1/S2 half-operator/promoter. Interaction of a 32 bp S1/S2 oligonucleotide (nt 571−602, Figure 1A) with increasing concentrations of SmtB has been investigated by the $g[s^*]$ analysis (*12*) of the boundary sedimentation velocity data. The superposition of the $g[s^*]$ analyses of the titration shows a continual increase in sedimentation coefficient of

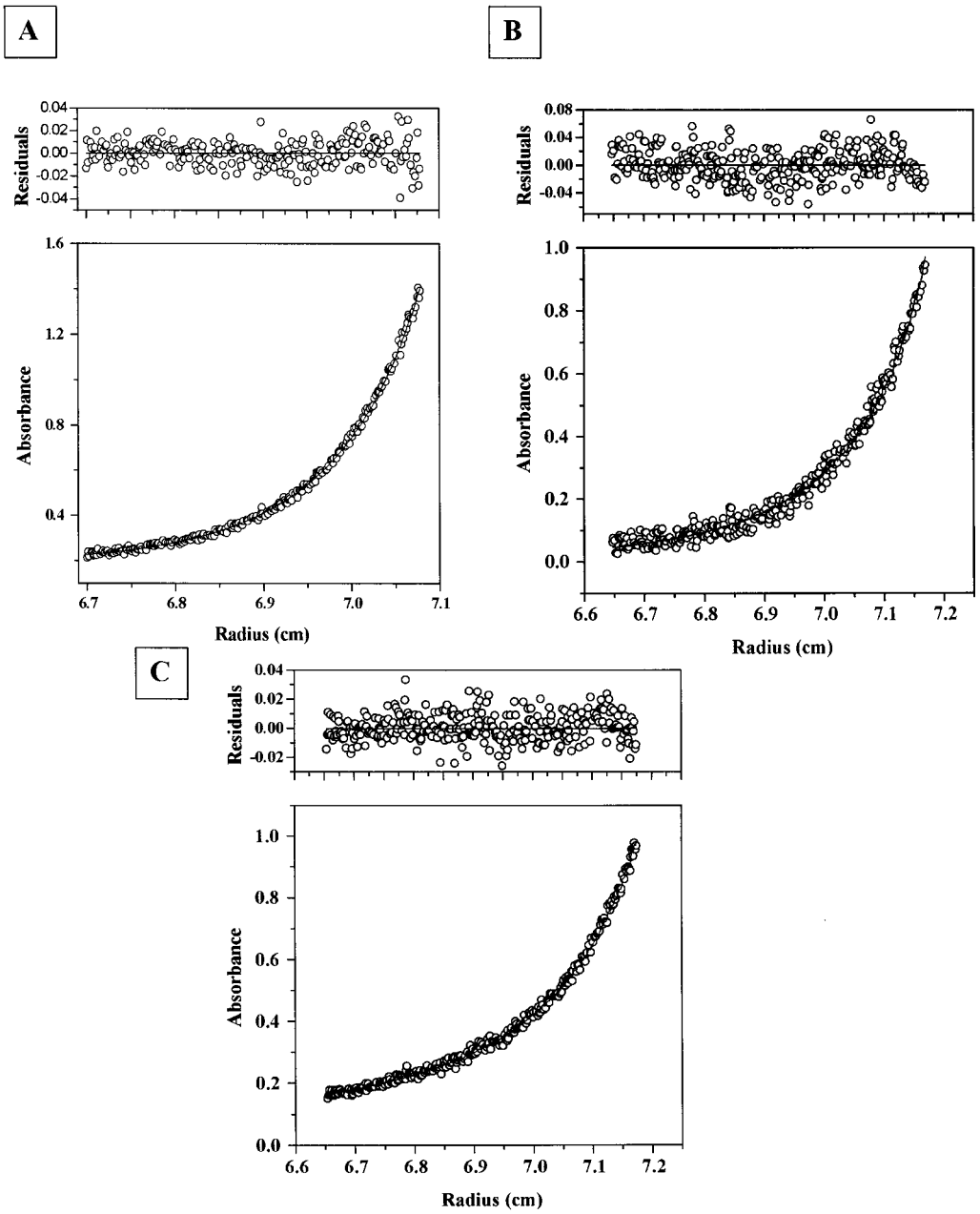

FIGURE 2: Sedimentation equilibrium analysis for the determination of SmtB binding stoichiometries. (A) Sedimentation equilibrium results of a mixture of 0.2 μM operator/promoter DNA and 8 μM SmtB; (B) sedimentation equilibrium results of a mixture of 0.35 μM S1/S2 DNA and 14 μM SmtB; (C) sedimentation equilibrium results of a mixture of 0.35 μM S3/S4 DNA and 14 μM SmtB. Lower Panels: Radial distribution of the concentration of the oligonucleotide (free and complexed with SmtB) at sedimentation equilibrium. The solid line through the points is the unweighted nonlinear least-squares fit for a single species. Upper Panels: Distributions of the residuals around a zero mean.

the resulting species from an initial value of 2.96 S for the free oligonucleotide to a final value of 7.20 S for the saturating complex (Figure 4A).

Comparison of the experimental *s* value at saturation with the theoretical $s_{20,w}$ values for nonhydrated spherical protein−DNA complexes with different binding ratios allows us to estimate the binding stoichiometry. Spherical nonhydrated complexes of 1:1, 1:2, and 2:2 DNA:dimer ratios would have $s_{20,w}$ values of 5.85, 7.35, and 9.31 S, respectively (*18*, *19*). The identity of the SmtB−S1/S2 complex at saturating protein concentrations can be deduced by comparing its experimental sedimentation coefficient (7.42 S) to the theoretically predicted value (7.35 S) for a complex composed of the 32 bp duplex and two SmtB dimers (Table 2). The agreement between the experimental $s_{20,w}$ value and the theoretical value for a hard sphere for the 1:2 S1/S2−SmtB complex indicates that there is no hydration of the complex based on eq 2. Since a complete loss of the water of hydration is unrealistic, it is likely that $s_{20,w}$ is high to some extent due to experimental errors. However, the agreement between hydrodynamic and sedimentation equilibrium stoichiometry under saturating protein concentration indicates that the 1:2 S1/S2−SmtB complex is very close to a spherical shape.

Boundary Sedimentation Analysis of SmtB Binding to the S3/S4 Half-Operator/Promoter. The interactions of SmtB with a 31 bp S3/S4 oligonucleotide (nt 542−572, Figure 1A) have been similarly investigated by the $g[s^*]$ analysis of boundary sedimentation velocity data from a titration of the

Table 1: Determination of Stoichiometries of SmtB Binding to the Oligonucleotides

macromolecular components	calculated MW[a]	estimated average mass[b]	proposed composition of complex
SmtB dimer	26820	−	−
S_1S_2	20800	−	−
S_3S_4	20150	−	−
S_1S_2 + *n*SmtB[c]	−	71771	S_1S_2 + 1.90 dimers
S_3S_4 + *n*SmtB[d]	−	70458	S_3S_4 + 1.88 dimers
S_1S_2 + S_3S_4 + *n*SmtB[e]	−	92575	S_1S_2 + 1.93 dimers + S_3S_4
operator/promoter DNA	65000	65968	−
operator/promoter + *n*SmtB[f]		116460	operator/promoter + 1.92 dimers

[a] Calculated from elemental composition. [b] Based upon sedimentation equilibrium centrifugation. [c−f] Sequence molar mass for $n = 2$ are 74 440, 73 790, 94 590, and 118 640, respectively.

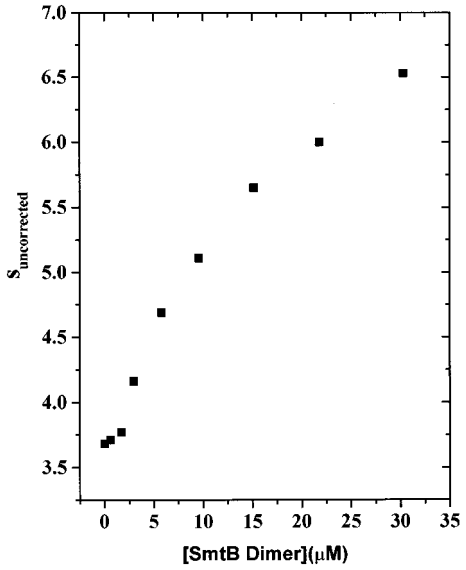

FIGURE 3: Data from the binding titration of the 100 bp operator/promoter DNA fragment with increasing molar concentrations of dimer SmtB calculated from the known SmtB association constants (*5*). The titration was done by the band sedimentation velocity technique, the details of which are described in the text. The experimental sedimentation coefficients of the DNA species (free and complexed) are the average of three experiments. The error in *s* for all measurements is ±0.07 S. The *s* values at each protein concentration are uncorrected for the effects of density and viscosity of 50% buffered D_2O.

oligonucleotide with increasing concentrations of the protein (Figure 4B). The *g*[*s**] analysis first shows a single *g*[*s**] distribution with increasing sedimentation upon titration of 1.5 μM S3/S4 oligonucleotide with increasing concentrations of SmtB from 6 to 21 μM. However, the addition of 25 and 30 μM SmtB generates bimodal *g*[*s**] distributions (Figure 4B). The value of the first *g*[*s**] peak value of 5.51 S corresponds very well to a theoretical value (*18, 19*) for an unhydrated spherical protein−DNA complex of 5.83 S (Table 2) composed of the S3/S4 duplex and one protein dimer. This interpretation is based on the same reasoning discussed above for the S1/S2−SmtB complex. The second peak value of 8.05 S is higher than the theoretically predicted value (*18, 19*) of 7.34 S for a 1:2 S3/S4−dimer complex. It is to be noted that the second Gaussian distribution increases in area at the expense of the first distribution; i.e., the first distribution peak is converted to higher molecular weight species with higher *s* values at the indicated SmtB concentrations shown in Figure 4B.

Table 2: Sedimentation Velocity and Hydrodynamic Characterization of the SmtB−DNA Complexes

SmtB−DNA complexes[a]	exptl $s_{20,w}$ value (S)	predicted $s_{20,w}$ of spherical protein−DNA complex	asymmetry factor (f/f_o)
complex near-saturation of band titration (1:2 DNA:dimer)	8.52	11.42	1.34
saturation peak of *g*[*s**] titration (1:2 S1/S2 DNA:dimer)	7.42	7.35	0.99
1st *g*[*s**] titration peak (1:1 S3/S4 DNA:dimer)	5.51	5.83	1.06
2nd *g*[*s**] saturation peak (multiple species)	8.05	−	−

[a] Complexes identified by sedimentation equilibrium (see Figure 2 and Table 1).

Obviously, there are distinctive differences in SmtB binding to S1/S2 DNA vs S3/S4 DNA. For the latter, binding appears restricted to 1:1 DNA−SmtB complex formation until 21−25 μM SmtB has been added to the S3/S4 DNA, and then a second *g*[*s**] distribution peak forms. For the S1/S2 titration, the initial incremental change in *s* at 6 μM SmtB is comparable to the change observed in the S3/S4 titration, suggesting an initial formation of 1:1 S1/S2−SmtB complex. However, the incremental changes in *s* increase rapidly for the S1/S2 titration, reflecting the formation of 1:2 S1/S2−SmtB complexes. Both hydrodynamic and sedimentation equilibrium analyses, described above, support the final formation of 1:2 DNA−SmtB complexes. However, there is only a single *g*[*s**] distribution for the S1/S2 titration, indicating that the 1:1 and 1:2 S1/S2−SmtB complexes are not separable by velocity sedimentation. One would expect a similar situation for the binding titration of the S3/S4 DNA if only 1:1 and 1:2 S3/S4−SmtB complexes were formed. What then accounts for the bimodal *g*[*s**] distributions? If the 1:2 S3/S4−SmtB complexes were capable of further interaction to form a higher molecular weight complex with slow dissociation rate constant(s) relative to the sedimentation velocity time, then boundary separation could occur. Consequently, we interpret the second *g*[*s**] peak to be a mixture of a 1:2 S3/S4−dimer complex and a higher molecular weight complex which has a sufficiently high *s* value to allow for separation of components, giving rise to the observed bimodal *g*[*s**] distributions. A nonhydrated spherical 2:2 DNA−dimer complex would have an $s_{20,w}$ value of 9.3 S (*18, 19*), suggesting that the second peak value of 8.05 S could be a mixture of the 1:2 and 2:2 DNA−dimer complexes. At the 4.28-fold lower S3/S4 DNA concentration used in the sedimentation equilibrium experiment, 2:2 DNA−dimer complexes could not have formed in appreciable amounts, since this would have been reflected in a much higher weight average molecular weight than observed. Evidently, higher concentrations of 1:2 DNA−SmtB complexes appear necessary to generate the putative S3/S4 2:2 DNA−SmtB complex. It would appear that a 1:2 S3/S4−SmtB complex interacts with another 1:2 S3/S4−SmtB complex or a 1:1 S3/S4−SmtB complex, and either two

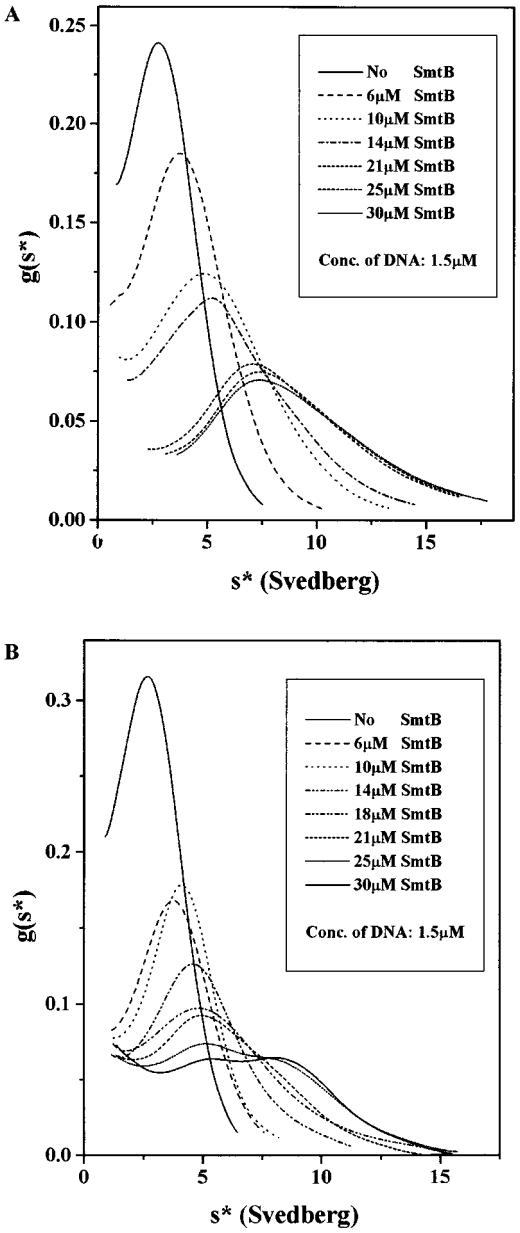

FIGURE 4: (A) Boundary sedimentation analysis of SmtB binding to S1/S2. Overlaps of the $g[s^*]$ distributions for the titration of the S1/S2 oligonucleotide with SmtB are shown here. The concentrations of the protein and the DNA are given in the inset. The sedimentation coefficient distributions show continual increase in the apparent s values (s^*), uncorrected for diffusion (*12*) with increasing protein concentrations until saturation is achieved. (B) Boundary sedimentation analysis of SmtB binding to S3/S4. Overlaps of the $g[s^*]$ distributions for the titration of the S1/S2 oligonucleotide with SmtB have been plotted here. The concentrations of the protein and the DNA are given in the inset. The sedimentation coefficient distributions clearly show a bimodal mechanism for binding to this oligonucleotide. The area under the second peak increases at the expense of the first.

dimers or one dimer becomes displaced to yield the S3/S4−SmtB:SmtB−S3/S4 complex. The latter "bridge" complex is stabilized by dimer−dimer interactions. Since we do not detect bridge complexes for the S1/S2 case, but do detect a 1:2 S1/S2 DNA−SmtB complex, it appears that it is the S3/S4 site that provides the capacity for the formation of bridge complexes. This opens the question whether a SmtB bridge complex can form between S1/S2 and S3/S4 oligonucleotides. To test this hypothesis, we performed the experiment described below.

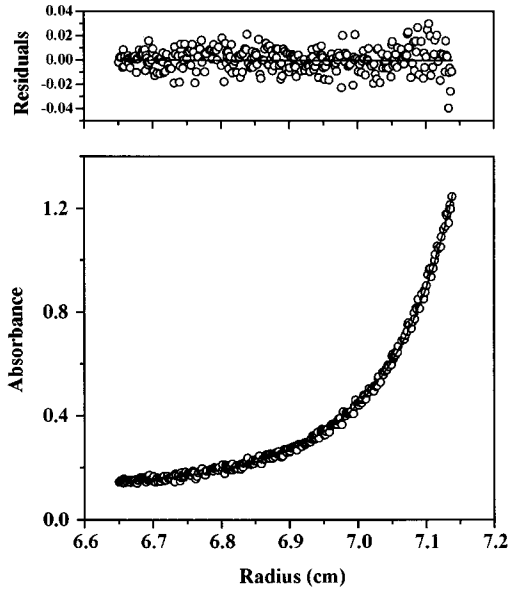

FIGURE 5: Sedimentation equilibrium analysis for the determination of the stoichiometry for SmtB binding to an equimolar mixture of S1/S2 and S3/S4 oligonucleotides. The sedimentation equilibrium data shown are for a mixture of 0.175 μM S1/S2 DNA and 0.175 μM S3/S4 plus 14 μM SmtB. Lower Panel: Radial distribution of the concentration of an equimolar concentration of the S1/S2 and the S3/S4 oligonucleotides (free and complexed with SmtB) at sedimentation equilibrium. The solid line through the points is the unweighted nonlinear least-squares fit for a single species. Upper Panel: Distributions of the residuals around a zero mean.

Binding of SmtB to the S1/S2 and S3/S4 Oligonucleotides Simultaneously. Sedimentation equilibrium analysis was used to determine whether equimolar mixtures of S1/S2 and S3/S4 oligonucleotides could also form a 2:2 DNA−dimer bridge complex in the presence of saturating levels of SmtB (Figure 5). These results show that the weight average molecular weight of the complex is 92 575 to give a DNA:dimer ratio of 2:1.93 (Table 1). As discussed above, we can envision the two duplexes (in this case S1/S2 and S3/S4) to be tethered together by two SmtB dimers. This result correlates with the hypothesis regarding the identity of the second $g[s^*]$ peak from the titration of the S3/S4 oligonucleotide with SmtB. It should be noted that this bridge complex forms at much lower DNA concentrations when S1/S2−SmtB and S3/S4−SmtB complexes are allowed to interact as opposed to when only S3/S4 sites are present. Such a complex of two duplex molecules held together by the two SmtB dimers can be considered as a mimic of the binding event with the whole operator/promoter DNA.

DNase I Footprint and Electrophoretic Mobility Shift Assay of SmtB Operator/Promoter Interactions. The generation of the footprints upon titrating a DNA fragment containing the *smt* operator/promoter region with SmtB is shown in Figure 6, panel A. The emergence of the footprints correlated with the formation of the different protein−DNA complexes by gel shift analysis (Figure 7) of aliquots of the same protein−DNA mixtures used for the footprint experiments (analyzed prior to the addition of the nuclease).

SmtB has a very well-defined footprint, bracketed on one end by the *smtB* −10 sequence and at the other, by the position 4 bp beyond the *smtA* Shine−Delgarno (S.D.)

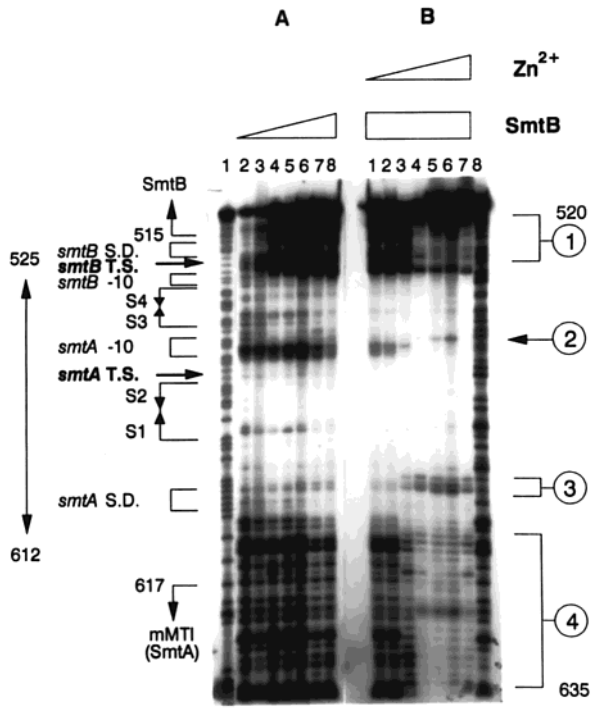

FIGURE 6: DNase I footprint of SmtB on a 141 bp fragment containing the *smt* operator/promoter region in the presence and in the absence of Zn^{2+}. Panel A: Lane 1, Maxam−Gilbert sequence of the fragment; lanes 2−8, ∼40 nM DNA with 0.05, 0.1, 0.2, 0.4, 1.6, 3.2, and 7.5 μM SmtB. Panel B: Lanes 1−7, complex C3 (similar to that in lane 8, panel A) treated with 0.0, 0.05, 0.25, 1, 5, 25, and 50 μM $ZnCl_2$; lane 8, control with ∼40 nM DNA + 50 μM $ZnCl_2$, no SmtB. The cleavage pattern of free DNA without $ZnCl_2$ was identical to that shown here. Abbreviations: S.D., Shine−Delgarno sequence; T.S., transcription start site; S1S2, S3S4, inverted repeats containing guanine residues identified by methylation interference assay (*2*); mMT1, mouse metallothionein.

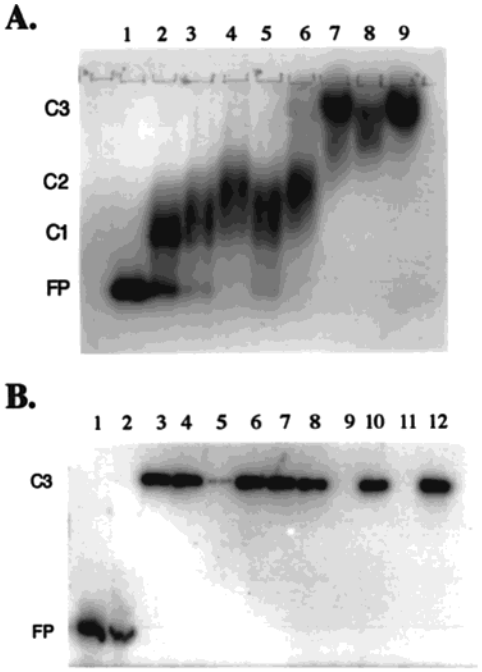

FIGURE 7: Gel shift analysis of SmtB−DNA C1, C2, and C3 complexes in the presence and absence of Zn^{2+}. (A) Lanes 1−9: 40 nM DNA probe + 0.0, 0.05, 0.1, 0.2, 0.4, 0.8, 1.6, 3.2, and 7.5 μM SmtB, respectively. SmtB−DNA complexes C1, C2, and C3 are indicated. (B) Lane 1, ∼40 nM DNA probe; lane 2, ∼40 nM free probe + 100 μM Zn^{2+}; lanes 3 and 4, C3 complex, no Zn^{2+}; lanes 6−8, 10, and 12, C3 complex with the addition of 0.25, 1, 10, 50, and 100 μM Zn^{2+}, respectively.

sequence (Figure 1A). The footprint is interrupted in the middle by a 4 bp region lying between the *smtA* −10 and the *smtA* transcription start (T.S.) sites. This 4 bp divider is more intense (signifying DNase I enhancement) compared to the bands at the same spot in the digestion pattern of the DNA by itself (lane 8 of panel B, Figure 6). A Maxam−Gilbert, A plus G, sequencing reaction of the DNA fragment is shown in lane 1 of panel A, Figure 6.

Interestingly, the footprint is distinctly visible even at the lowest protein concentration used. From the difference in intensity of the two halves of the footprint, it is clear that the lower half (the S1/S2 locus) of the footprint emerges prior to the upper half (the S3/S4 locus) with increasing protein concentrations. This observation again supports a sequential binding event. Essentially, a complete footprint is obtained at the indicated protein concentrations (lanes 2−5 of panel A, Figure 6) when only the first two protein−DNA complexes (C1 and C2) are being formed (lanes 2−6, Figure 7A).

The effect of increasing concentrations of Zn^{2+} ions on preformed C3 complex at saturating protein concentration (7.5 μM) was analyzed by both DNase I footprinting (lanes 1−7 of panel B, Figure 6) and gel shift (lanes 1−12, Figure 7B) assays. From the gel shift assay, it is apparent that the complex C3 does not dissociate with the addition of Zn^{2+}. This observation is corroborated by the persistence of the protein footprint on the DNA in the presence of metal ions. What is to be noted, however, is that there seems to be a threshold for the metal ion (around 0.25 μM, lane 3 of panel B, Figure 6) above which the footprint patterns expand as well as exhibit changes. At metal concentrations ≥0.25 μM, the footprint extends almost the entire length of the DNA fragment, extending beyond the *smtB* −10 region into the *smtB* coding region on one end (demarcated by the bracket labeled 1, Figure 6) and into the *mMT1* coding region at the other end (demarcated by the bracket labeled 4, Figure 6). This extension of the footprint is accompanied by the following changes in the cleavage pattern: (1) the divider bands separating the two halves of the footprint (lanes 2−8 of panel A, Figure 6) disappear above the threshold concentration of the metal and are replaced by a single band just above them (denoted by the arrow labeled 2, Figure 6); and (2) the patterns demarcated by the bracket labeled 3 (Figure 6) intensify with increasing metal ion concentration. The enlargement of the footprint is not caused by any additional SmtB binding to DNA, since it has already been shown that the metal-bound protein is incapable of interacting with DNA (*1*, *2*).

DISCUSSION

We have examined, using a combination of experimental approaches, SmtB binding to both the entire promoter/operator DNA and the separate S1/S2 and S3/S4 operator sites in order to develop a working model of the SmtB binding interactions that lead to a functional repression complex. In addition, we have examined the validity of the generally accepted model that Zn^{2+} binding to SmtB causes the protein to dissociate from DNA, allowing activation of

transcription of the metallothionein gene. We believe that the results reported in this study combined with the results obtained from an earlier binding interference analysis (*2*) allow us to propose a model for the formation of the SmtB repression complex and a plausible mechanism underlying the Zn^{2+}-inducible regulation of the *smt* locus by SmtB.

The final stoichiometry of SmtB binding to the whole 100 bp operator/promoter is two dimers to one DNA molecule, i.e., one SmtB dimer interacting with each of the operator sites. The SmtB binding interference data of DNA isolated from the slowest gel-retarded complex (C3) identified SmtB contact interactions with the S1/S2 and S3/S4 sequences (*2*). This result is corroborated by the extensive protection from DNase I cleavage as seen for both the S1/S2 and S3/S4 regions for the C3 complex (Figure 6A). If the C3 complex is the final repression complex, can we account for the nature of the C1 and C2 complexes? After all, if two dimers of SmtB are binding sequentially, then we ought to observe the formation of only two electrophoretic species in gel retardation assay, and not three.

Sedimentation velocity and equilibrium analysis of the 32 bp S1/S2 DNA supports the binding of two dimers. A reasonable model that one can consider involves binding of two SmtB dimers to the S1/S2 site of the whole operator/promoter, followed by a "transfer" of one of the dimers to the S3/S4 site to generate the repression complex. Binding interference analysis of the intermediate migrating complex C2 showed that both the S1 and S2 sites are contacted by SmtB, and modification of the G residue in the S3 sequence partially interferes with C2 complex formation (*2*). This result suggests a transfer process; however, conversion of C2 to C3 is SmtB concentration-dependent (Figure 7A), and consequently a simple "transfer" model will not suffice to account for the observed results. If there are two dimers bound in the C2 complex (at S1/S2) and in the C3 complex (at S1/S2 and S3/S4), what accounts for the electrophoretic differences of the complexes and the concentration-dependent conversion of C2 to C3? The $s_{20,w}$ of the SmtB−operator/promoter complex is 8.52 S, which gives an asymmetry factor (f/f_o) of 1.34 (Figure 3, Table 2). It should be emphasized that this is a conservative estimate of the f/f_o based on the last data point of the titration of Figure 3. We did not use an extrapolation to the mathematical plateau value which would have given us a more compact SmtB−DNA complex. As indicated earlier, we can model the 1:2 operator/promoter−SmtB complex as a prolate ellipsoid of revolution with major and minor axial dimensions of 18.35 and 4.43 nm, respectively. The full length of the free 100 bp operator/promoter DNA is 34 nm. To account for the observed hydrodynamic behavior, the DNA in the 1:2 operator/promoter−SmtB complex has to have a reduced effective length due to SmtB binding interactions. Bending of the DNA would reduce the effective hydrodynamic volume of a protein−DNA complex from rod or cylinder shape to a shape that can be approximated by a prolate ellipsoid. Hence, we propose that C3 has a lower electrophoretic mobility, i.e., greater mobility retardation, because of DNA bending induced by SmtB interactions. Both S1/S2 and S3/S4 half-operators are capable of forming 1:2 DNA−SmtB complexes. However, when S1/S2 and S3/S4 half-operator DNAs are mixed in equal molar concentration, in excess SmtB, a S1/S2:SmtB:SmtB:S3/S4 "protein bridge" complex forms.

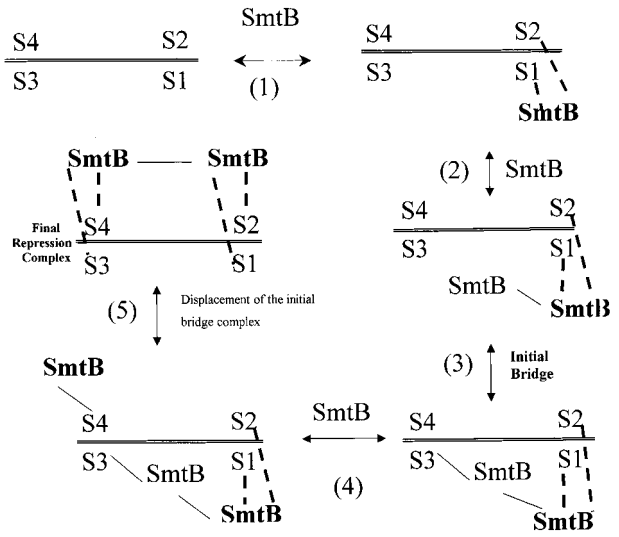

FIGURE 8: Cartoon depicting the sequential binding of SmtB dimers to form the final repression complex. This pictorial representation, which does not indicate any structural details, is meant to be a visual aid to describe the proposed multistep (numbered 1 through 5) binding scheme. The details of the scheme are given in the text. The SmtB dimers shown in boldface letters are the ones that, upon making contact interactions with DNA, are never released. These are in contrast to the bridge dimer that is displaced in step 5. The interactions denoted by the boldface dashed lines represent the binding of the protein dimer to both halves of the inverted repeats by HTH interactions. Step 1 results in the formation of the electrophoretic species C1. The complex C2 is formed after step 3 when the initial bridge is being created. The final electrophoretic species C3 results following step 5, the displacement of the initial bridge SmtB. The new positions of SmtB are not intended to indicate any translocation events but were required for space considerations.

The reaction of either 1:1 S3/S4−SmtB or 1:2 S3/S4−SmtB complex with a 1:2 S1/S2−SmtB complex occurs to form a 2:2 DNA(half-operator)−SmtB complex with the release of either one or two dimers.

We have developed a sequential SmtB binding model for the formation of the final SmtB−operator/promoter repression complex based on the results reviewed above coupled with previous binding interference data (*2*). To assist the reader in following the sequential steps of SmtB binding, a pictorial representation is provided in Figure 8. Binding of a SmtB dimer initially occurs at the S1/S2 site by helix−turn−helix interactions of each subunit with each inverted repeat sequence (Figure 8, step 1). This 1:1 S1/S2−SmtB corresponds to the C1 electrophoretic complex. As the SmtB concentration is raised, a second dimer binds to the 1:1 S1/S2−SmtB complex to yield a 1:2 DNA−SmtB complex at S1/S2 (Figure 8, step 2). This second dimer is first stabilized by protein−protein interactions. DNA isolated from the C2 complex shows missing bands (binding interference sites) at S1/S2 and a significantly diminished band at S3 but not S4 (*2*). The combined interference data (*2*) and footprinting data (Figure 6, panel A) indicate that contact interactions also occur with the S3/S4 region in the C2 complex. Since the sedimentation data show that two dimers can bind at S1/S2, we propose that the C2 electrophoretic entity is a "bridge" complex of two dimers between S1/S2 and the S3 recognition sequence (Figure 8, step 3). We designate the second S1/S2-bound dimer, which contacts S3, as the initial protein bridge and propose that one subunit is brought

into position for the helix−turn−helix binding domain to interact with the S3 recognition sequence. The distance from the S2 recognition site to the S3 half-site is 54 Å, and the length of the dimer is 68 Å (*6*). Induced DNA bending could be involved to allow the bridge dimer to interact with the S3 site. The bridge dimer is constrained by interactions with the S1/S2-bound dimer, and this prevents the HTH domain of the free subunit from making contact interactions with S4. However, upon further addition of SmtB, another dimer becomes bound at S4 (Figure 8, step 4). Since the S3 site is blocked by the initial bridge dimer, only one monomer of the third dimer can interact with DNA with the formation of a transient intermediate complex with a dimer at S4 and the bridge dimer at S3. Since binding at S4 occurs with only one subunit of the SmtB dimer, the association constant for this interaction is probably low, requiring a large excess of SmtB to obtain significant binding. However, once S4 binding has occurred, a free subunit is available to compete for the S3 site with the bridge dimer. We now propose displacement of the initial bridge dimer by the S4 dimer to form C3 with very fast kinetics (Figure 8, step 5). We envision that this occurs by the HTH domain of the free subunit of the S4 dimer displacing the DNA recognition domain of the S3 bridge subunit followed by the formation of new more stable bridge interactions with the S1/S2 dimer and the release of the initial bridge dimer. This displacement process occurs in concert with further bending of the DNA and stabilization of the bending through the bridging protein−protein interactions between the S1/S2 and S3/S4 dimers. This final C3 repression complex has slower electrophoretic mobility due to DNA bending. The direction of the bending could orient different interaction surfaces of SmtB, promoting a more stable bridge structure.

The separation of the two pairs of sites is 17 bp (Figure 1A). This distance may be too short to loop-out this segment of the DNA to bring the two pairs of sites in juxtaposition, as seen with AraC (*20*) and Lac (*21*) repressors. But this 17 bp segment could be bent by SmtB through a large angle. Recently, it has been shown that the *Chironomus* HMG1a protein bends a 30 bp DNA through an angle of 150° in addition to untwisting the double helix through 90° (*22*). A similar mechanism may well be at play in the case of SmtB binding to its cognate DNA.

Although the above model accounts for the observed sedimentation, electrophoretic, and binding interference results, considerable details are missing, and there are many questions that need to be addressed. From a qualitative perspective, both binding interference analysis and footprinting data of the entire operator/promoter support the sequential occupancy of S1/S2 before S3/S4, yet binding titrations to half-operators indicate that the initial binding of the first SmtB dimer to each respective half-operator site occurs with comparable affinity. The mechanism for highly preferential SmtB binding to S1/S2 vs S3/S4 for the entire operator/promoter is not clear. However, the sequential binding process appears to be necessary to establish the final C3 repression complex. For the C3 complex, a single G modification in any of the HTH recognition sites completely disrupts the formation of this complex, possibly caused by disrupted dimer stability at either pair of sites (2). The linkage of SmtB dimers through a bridge complex would account for this observed G modification interference result. It should be mentioned again that free SmtB is capable of weak tetramerization (*5*). Obviously, it would be of considerable value to quantitatively determine the multiple association constants for the steps in the binding process that are shown in the reaction scheme of Figure 8. The ability to computationally model such a complex binding equilibria is a difficult problem beyond the scope of this paper. The frictional ratios for the half-operator 2:1 S1/S2−SmtB complex and the 1:1 S3/S4−SmtB complexes are essentially unity, indicating a highly spherical shape for these complexes. However, free SmtB dimers are asymmetric with an f/f_o of 1.42, consistent with the crystal structure of the dimer (*5*, *6*). These hydrodynamic data suggest major conformational changes in SmtB upon binding DNA.

The structure of the SmtB dimer shows two putative "winged" helix−turn−helix DNA binding domains, one in each subunit (*6*). A DNA recognition helix is at the end of each monomer. There is structural similarity between the DNA binding domains of SmtB, CAP, and HNF-3 (*6*). To attempt to model the interactions of SmtB with DNA, the HTH domains of SmtB were superimposed onto the corresponding structures of CAP and HNF-3 complexed with DNA. For the CAP alignment, simultaneous binding of DNA to both ends of the dimer would require a bend of over 120° in the DNA helix (*6*). Using HNF-3 for the alignment would allow DNA binding to both ends with only a 30° DNA bend (*6*). As pointed out above, large DNA bending would account for a more retarded C3 electrophoretic complex and the frictional asymmetry obtained from the sedimentation velocity data. We have proposed that the DNA bending is stabilized by SmtB−SmtB bridge interactions in the final repression complex. We envision that this compact SmtB−operator/promoter complex would not be accessible to RNA polymerase, thereby blocking SmtA transcription.

Since we demonstrated that Zn^{2+} does not dissociate SmtB from the C3 complex, it would appear that Zn^{2+} binding induces conformational changes in SmtB to promote RNA polymerase accessibility. If the SmtB bridge interactions are disrupted, and bending relieved, one could envision that SmtB would be converted into a transcription activator of SmtA. The footprint of the repressor enlarges with increasing concentrations of the metal ion and extends into the metallothionein coding region. The new SmtB−DNA interactions promoted by the Zn^{2+}-induced conformational changes seem to affect the minor groove of DNA, reducing DNase I nuclease accessibility. The bacterial MerR repressor, which regulates the mercury-detoxification genes, can switch between repressor and activator modes without dissociating from the DNA (*23*). This switching from the repressor to the activator mode is accomplished via stereospecific structural modulation of the DNA. Recently, the gene product ZntR has been identified that regulates the transcription of the gene coding for a Zn^{2+} export protein, ZntA, in *Escherichia coli* (*24*). ZntR has been shown to act as a hypersensitive Zn^{2+}-inducible transcriptional switch with MerR-like properties (*24*). Arguably, SmtB may also have such dual functionality whereby it represses the *smt* locus in the uninduced state while switching over to an activator mode in the presence of heavy metal ions.

Regulation of transcription often involves the assembly of multiprotein complexes, and interactions between adjacent and nonadjacent DNA binding proteins can enhance the

specificity and stability of nucleoprotein complexes (*25*). For example, the binding of CAP and Lac repressor to their recognition sequences can be enhanced by HU protein in vitro, although HU does not appear to be present in the final protein−DNA complex (*26*). Very recently (*27*), a study of HU−DNA binding interactions found up to five protein−DNA complex bands in gel mobility shift assays whereas stoichiometric analysis by both sedimentation equilibrium and fluorescence anisotropy revealed only three bound HU molecules at saturation. It was suggested that protein-induced bending of the DNA leads to the observation of electrophoretic complexes in the gel, which have the same molecular weight but different relative mobilities (*27*). These HU results and the bending hypothesis are in support of our model to account for the electrophoretic difference between the C2 and C3 bands observed in our gel shift assay. The proposed working model for SmtB−DNA and SmtB bridging interactions for generating a repression complex and the role Zn^{2+} may play provide a framework for further analysis of SmtB−operator/promoter interactions and the development of a more in-depth understanding of transcriptional control of the synechococcal metallothionein locus.

ACKNOWLEDGMENT

We sincerely thank Dr. Charles Turnbough at UAB for being such an invaluable source of extensive knowledge and expertise in the field of transcriptional regulation of cellular processes. We also thank Drs. Marc S. Lewis and Peter Schuck at NIH for their expert advice and guidance in analytical ultracentrifuge methodologies.

SUPPORTING INFORMATION AVAILABLE

Reproduction of Figure 5 from Erbe et al. (*2*) (2 pages). This material is available free of charge via the Internet at http://pubs.acs.org.

REFERENCES

1. Morby, A. P., Turner, J. S., Huckle, J. W., and Robinson, N. J. (1993) *Nucleic Acids Res. 21*, 921−925.
2. Erbe, J. L., Taylor, K. B., and Hall, L. M. (1995) *Nucleic Acids Res. 23*, 2472−2478.
3. Huckle, J. W., Morby, A. P., Turner, J. S., and Robinson, N. J. (1993) *Mol. Microbiol. 7*, 177−187.
4. Turner, J., and Robinson, N. J. (1995) *J. Ind. Microbiol. 14*, 119−125.
5. Kar, S. R., Adams, A. C., Lebowitz, J., Taylor, K. B., and Hall, L. M. (1997) *Biochemistry 36*, 15343−15348.
6. Cook, W. J., Kar, S. R., Taylor, K. B., and Hall, L. M. (1998) *J. Mol. Biol. 275*, 337−346.
7. VanZile, M. L., Cosper, N. J., Scott, R. A., and Giedroc, D. P. (2000) *Biochemistry 39*, 11818−11829.
8. Kosada, T., Morita, E. H., Miura, A., Yamazaki, T., Hayashi, H., and Kyogoku, Y. (1999) *J. Biomol. NMR 14*, 191−192.
9. Silver, S., and Phung, L. T. (1996) in *Annual Review of Microbiology* (Ornston, L. N., Ed.) pp 753−789, Annual Reviews, Inc., Stanford, CA.
10. Turner, J. S., Glands, P. D., Samson, A. C. R., and Robinson, N. J. (1996) *Nucleic Acids Res. 24*, 3714−3721.
11. Vinograd, J., Bruner, R., Kent, R., and Weigle, J. (1963) *Proc. Natl. Acad. Sci. U.S.A. 49*, 902−910.
12. Stafford, W. F., III (1992) in *Analytical Ultracentrifugation in Biochemistry and Polymer Science* (Harding, S. E., Rowe, A. J., and Horton, J. C., Eds.) pp 359−393, The Royal Society of Chemistry, Cambridge, U.K.
13. Bailey, M. F., Davidson, B. E., Minton, A. P., Sawyer, W. H., and Howlett, G. J. (1996) *J. Mol. Biol. 263*, 671−684.
14. Woodward, R. S., and Lebowitz, J. (1980) *J. Biochem. Biophys. Methods 2*, 307−309.
15. Ausubel, F. M., Brent, R., Kingston, R. E., Moore, D. D., Seidman, J. G., Smith, J. A., and Struhl, K. (1994) *Current protocols in molecular biology*, John Wiley & Sons, New York.
16. Leblanc, B., and Moss, T. (1994) in *DNA−Protein Interactions: Principles and Protocols* (Kneale, G. G., Ed.) pp 1−10, Humana Press, Totowa, NJ.
17. Lebowitz, J., Kar, S., Braswell, E., McPherson, S., and Richard, D. L. (1994) *Protein Sci. 3*, 1374−1382.
18. Teller, D. C., Swanson, E., and De Haen, C. (1979) in *Methods in Enzymology: Enzyme Structure Part H* (Hirs, C. H. W., and Timasheff, S. N., Eds.) pp 103−124, Academic Press, Inc., New York.
19. Kumosinski, T. F., and Pessen, H. (1985) in *Enzyme Structure, Part J* (Hirs, C. H. W., and Timasheff, S. N., Eds.) pp 154−182, Academic Press, Inc., Orlando, FL.
20. Lobell, R. B., and Schleif, R. F. (1990) *Science 250*, 528−532.
21. Lewis, M., Chang, G., Horton, N. C., Kercher, M. A., Pace, H. C., Schumacher, M. A., Brennan, R. G., and Lu, P. (1996) *Science 271*, 1247−1254.
22. Heyduk, E., Heyduk, T., Claus, P., and Wisniewski, J. R. (1997) *J. Biol. Chem. 272*, 19763−19770.
23. Ansari, A. Z., Bradner, J. E., and O'Halloran, T. V. (1995) *Nature 374*, 371−375.
24. Brocklehurst, K. R., Hobman, J. L., Lawlwy, B., Blank, L., Marshall, S. J., Brown, N. L., and Morby, A. P. (1999) *Mol. Microbiol. 31*, 893−902.
25. Grosschedl, R. (1995) *Curr. Opin. Cell Biol. 7*, 362−370.
26. Flashner, Y., and Gralla, J. D. (1988) *Cell 54*, 713−721.
27. Wojtuszewski, K., Hawkins, M. E., Cole, J. L., and Mukerji, I. (2001) *Biochemistry 40*, 2588−2589.

BI011289F